Transported Probability Density Function Based Modelling of Soot Particle Size Distributions in Non-Premixed Turbulent Jet Flames

M. A. Schiener, R. P. Lindstedt*

Department of Mechanical Engineering, Imperial College, Exhibition Road, London SW7 2AZ, UK

Abstract

The need to establish actual particle size distributions (PSDs) of soot emissions from the nanoscale upwards, along with the current global indicators based on soot mass, stems from increasingly strict regulatory demands. In the current work, a mass and number density preserving sectional model is coupled with a transported probability density function (PDF) method to study the evolution of soot PSDs in two non-premixed turbulent jet flames at Reynolds numbers of 10,000 and 20,000. The transported PDF approach is closed at joint-scalar level and includes mass fractions of gas phase species, soot sections, as well as enthalpy, leading to a fully coupled 78-dimensional joint-scalar space, treating interactions between turbulence and gas phase/soot chemistry as well as radiation without further approximation. The gas phase chemistry features 144 reactions, 15 solved and 14 steady-state species and an acetylene-based soot inception model is calibrated using comprehensive detailed chemistry up to pyrene and applied to

*Corresponding author:
Email address: p.lindstedt@imperial.ac.uk (R. P. Lindstedt)

a well-stirred/plug flow reactor configuration. The derived nucleation rate is subsequently applied in the turbulent flame calculations. Soot surface growth is treated via a PAH analogy and oxidation via O, OH and O_2 is accounted for. The sectional model features 62 sections covering particle sizes in the range 0.38 nm $\leq d_p \leq$ 4.4 μm and includes a model for the collision efficiency of small particles ($\leq$ 10 nm) based on the Lennard–Jones potential. The computed results reproduce the evolution of the PSDs with encouraging accuracy. It is also shown that the distribution of soot in mixture fraction space is affected by local extinction events.

Keywords:
Particle size distributions, Turbulent flames, Transported PDF methods, Nucleation rates, Soot surface chemistry

---

Supplemental Material is available.

1. Introduction

The ability to model the dynamic evolution of soot particle size distributions (PSDs) from the soot inception limit in premixed systems to diffusion flame conditions is of fundamental importance in the light of increasingly stringent regulations on particulate emissions. This stems from the need to establish actual PSDs from the nanoscale upwards along with the current global indicators based on soot mass. Sectional models allow the solution of population balance equations (PBEs) and there is a corresponding need to formulate mass and number density conserving models. To date, such models have been developed and evaluated for laminar flames and simplified reactor geometries. A mass conserving sectional approach was developed by

Smooke et al. [1], and Wen et al. [2] used a moving sectional approach. Bhatt and Lindstedt [3] developed a fixed sectional method and studied soot in the combined well-stirred (WSR) and plug flow (PFR) reactor configuration of Manzello et al. [4]. The model was further applied to the PFR system of Kronholm and Howard [5, 6]. The WSR/PFR setup was studied by Lindstedt et al. [7] considering further experimental work [8] and introducing updated thermodynamical data for polyaromatic hydrocarbons (PAHs). The method was extended [9] in a study of the premixed laminar stagnation flow flames of Abid et al. [10–12] to include a model for the coagulation efficiency of small (< 10 nm) particles [13] based on the Lennard–Jones potential.

Moment methods [14] transport a finite set of moments of the particle size distribution function, rather than attempting a direct solution of the discretised PSD. Such approaches are computationally less expensive, making them the choice for turbulent flame calculations to date. Lindstedt and Louloudi [15] used a transported probability density function (PDF) approach [16] and the method of moments with interpolative closure (MOMIC) [17] to study soot formation in the turbulent diffusion flames by Kent and Honnery [18] and Coppalle and Joyeux [19]. A number of alternative strategies for the reconstruction of the PSD in the context of moment methods have been developed, leading to the quadrature [20], direct quadrature [21], hybrid [22, 23], conditional quadrature [24] and the extended conditional quadrature method of moments [25].

By contrast, sectional methods that provide the full PSD have not been evaluated in terms of their ability to reproduce experimental data from turbulent flames. The current work removes this limitation by the inclusion of

the sectional model of Lindstedt and Waldheim [9] into a transported probability density function approach that permits the inclusion of direct chemistry effects. The overall model is fully coupled to the gas phase chemistry and evaluated against the data sets of Boyette et al. [26] and Chowdhury et al. [27].

2. Model

2.1. Sectional Soot Model

The current mass and number density preserving sectional approach has been used in previous studies to compute soot particle size distributions in WSR/PFR configurations [3, 5, 7] and laminar flames [9]. Here, a size range up to 4.4 μm was covered by using a mass-based distribution of 62 soot sections with a geometric spacing factor $f_s = 1.5$ for particles in the range 0.48–100 nm that is gradually relaxed to 2.0 for larger particles. The upper particle size limit was selected to go beyond the experimental particle size range (2–225 nm). The rates of soot nuclation, growth and oxidation are shown in Table 1. Schiener and Lindstedt [28] explored the sensitivity to the soot nucleation rate by combining transported PDF and moment-based methods to calculate a turbulent non-premixed natural gas flame. A scaling factor of 3.75 was derived to provide consistency between simplified acetylene [15, 34] and pyrene-based (A_4, $d_{p,A_4} = 0.38$ nm) nucleation featuring a first order reaction in the acetylene concentration as for Eqs. (1)–(2).

$$8\ C_2H_2 \longrightarrow A_4 + 3\ H_2 \tag{1}$$

$$R_N = k_N(T)\,[C_2H_2] \tag{2}$$

The thermochemical properties of pyrene, determined at the G4MP2 and G3MP2B3 levels of theory [9], were assigned to the incipient soot particles. The rate of nucleation was derived by comparing the predicted PSDs obtained in a WSR/PFR configuration with comprehensive PAH chemistry and with the above simplified expression as discussed in Sec. 2.3. The acetylene-based nucleation model allows removal of gas phase PAH reactions with the number of solved species reduced from 359 [9, 29] to 15 [15] and a three order of magnitude reduction in computational cost.

The rate of soot growth is modelled via Eq. (3), where A_s is the soot surface area per unit volume.

$$R_G = k_G(T)\chi_s A_s \left[\mathrm{C_2H_2}\right] \tag{3}$$

$$\chi_s = \alpha_s \Psi(T, \phi_k) \frac{\chi_{s-h}}{N_A} \tag{4}$$

Lindstedt and Louloudi [15] derived the naphthalene-based analogy for soot surface growth shown in Eq. (4), where $\Psi(T, \phi_k)$ is obtained as a function of temperature (T) and gas composition (ϕ_k) from truncated steady-state approximations (see supplemental material), $\chi_{s-h} = 2.32 \times 10^{19}$ m^{-2} is the number of hydrogen sites per unit surface area and $N_A = 6.022 \times 10^{26}$ kmol^{-1} is Avogadro's number. The parameter α_s in Eq. (4) denotes the fraction of sites available for hydrogen abstraction. It varies as a function of the reaction history and models based on the thermal age of soot particles in laminar flames have been proposed [30–32]. The choice of a constant mean value is common and depends on other model aspects as well as the flame configuration [15, 33–36]. The approach has been adopted in the current work with $\alpha_s = 0.50$, higher than that used by Lindstedt and Waldheim [9] ($\alpha_s = 0.20$), but within the range proposed by Kazakov et al. [35] ($0.35 \leq$

Table 1: Rate constants for soot nucleation ($k_N = k_{N,3}/3.75$ [28]), growth (k_G) and oxidation via OH (k_{OH}), O (k_{O}) and O_2 ($k_{\mathrm{O_2}}$) in the form $A_i \alpha_i T^{\beta_i} \exp(-E_i/RT)$ [37–39]. Units are in K, kmol, m^3 and s.

k_i	A_i	α_i	β_i	E_i/R
k_N	1.68×10^1	1	0	21,000
k_G	3.57×10^{21}	1	-3.176	7,471
k_{OH}	8.82	0.10	1/2	0
k_{O}	9.09	0.20	1/2	0
$k_{\mathrm{O_2}}$	6.43	116	1/2	19,680

$\alpha_s \leq 0.60$) in the context of a method of moments approach for premixed laminar flames. A sensitivity analysis covering the range $\alpha_s = 0.50 \pm 0.20$ was accordingly performed. Soot oxidation is modelled via Eqs. (5)–(8).

$$\mathrm{C_{soot}} + \mathrm{OH} \longrightarrow \mathrm{CO} + \mathrm{H} \tag{5}$$

$$\mathrm{C_{soot}} + \mathrm{O} \longrightarrow \mathrm{CO} \tag{6}$$

$$\mathrm{C_{soot}} + \mathrm{O_2} \longrightarrow \mathrm{CO} + \mathrm{O} \tag{7}$$

$$R_O = \left(k_{\mathrm{OH}}(T)\,[\mathrm{OH}] + k_{\mathrm{O}}(T)\,[\mathrm{O}] + k_{\mathrm{O_2}}(T)\,[\mathrm{O_2}]\right) A_s \tag{8}$$

The molecular oxygen rate used in previous work [3, 15] was based on a study of carbon black oxidation by Roth et al. [38]. A rate with an increased barrier of 164 kJ/mol [34] for O_2, approaching the 195 kJ/mol proposed by Guo et al. [39], was used along with collision efficiencies for OH of 0.10 [38, 39] and 0.20 for O [38]. Oxidation and surface growth in the 0th bin can be treated as for pyrene (A_4), but is here neglected for simplicity. Particles are considered spherical, and coagulation in the free molecular, continuum and transition regimes is modelled as a function of the Knudsen number ($\mathrm{Kn} = 2\lambda/d_p$),

based on the mean free path (λ) and the soot particle diameter (d_p) [3].

Lindstedt and Waldheim [9] modelled the size dependent particle collision efficiency following Narsimhan and Ruckenstein [13], where the lower limit was derived based on the Lennard–Jones potential, assuming friction with the surrounding medium to be negligible. The corresponding collision efficiency (α_e^l) in the free-molecular regime is,

$$\alpha_e^l = 1 - \left(1 + \frac{\Phi_0}{k_b T \theta}\right) \exp\left(-\frac{\Phi_0}{k_b T \theta}\right) \tag{9}$$

$$\theta = 1 + \frac{2\Phi_0}{3 k_b T} \tag{10}$$

where Φ_0 denotes the potential well depth, k_b is the Boltzmann constant and θ is the dimensionless surface temperature given by Eq. (10). The upper limit (α_e^u) for sufficiently large particles is set to unity [9]. The coagulation rate in the free-molecular regime is,

$$\begin{aligned}\beta_{i,j}^{C,f} = C_a \alpha_e \left(\frac{3}{4\pi}\right)^{1/6} \left(\frac{6 k_b T}{\rho_s}\right)^{1/2} \left(\frac{1}{v_i} + \frac{1}{v_j}\right)^{1/2} \\ \times \left(v_i^{1/3} + v_j^{1/3}\right)^2\end{aligned} \tag{11}$$

where $C_a = 3.0$ [9] is the van der Waals enhancement factor, v_i denotes the volume of particles in the ith soot section and $\rho_s = 1800$ kg/m^3 is the soot density. The parameter α_e denotes the collision efficiency, calculated from the lower and upper bounds using a blending function (f_i),

$$\alpha_e = \left(f_i f_j\right)^{1/2} \alpha_e^u + \left(1 - \left(f_i f_j\right)^{1/2}\right) \alpha_e^l \tag{12}$$

$$f_i = \frac{1}{2}\left(\tanh A^* \left(d_{p,i} - D\right) + 1\right) \tag{13}$$

where D is the particle diameter at which the lower bound starts becoming insignificant and $A^* = \ln(\alpha_{e,\mathrm{A}_4}/(100 - \alpha_{e,\mathrm{A}_4}))/(2d_{p,\mathrm{A}_4} - 2D)$ is defined so that

the influence of the upper bound on pyrene is negligible [9]. Lindstedt and Waldheim [9] proposed a functional form for the upper bound D, based on the maximum flame temperature in laminar premixed C_2H_4 flames [10–12], resulting in values in the range $2.5 \leq D \leq 6$ nm. Narsimhan and Ruckenstein [13] and D'Alessio et al. [40] suggest the upper bound to be close to or above 6 nm. A condition dependent increase of the rate of internal carbonisation with temperature was proposed as a possible explanation for discrepancies between different studies [9]. In the current work, the sensitivity to D is explored for the range $2 \leq D \leq 6$ nm (see Sec. 3). The Hamaker constant determines the potential energy well-depth Φ_0, and a lower limit value of 7.0×10^{-20} J for non-carbonised particles is used [9]. This is somewhat higher than the value for benzene (5.0×10^{-20} J) applied by D'Anna and Kent [41] and the lower limit value of 3.0×10^{-20} J by D'Alessio et al. [40]. A sensitivity analysis for values in the range 3.0×10^{-20} to 7.0×10^{-20} J was performed (see Sec. 3).

2.2. Transported PDF Method Implementation

Lindstedt et al. [15, 42, 43] coupled a two-dimensional implicit Reynolds-averaged Navier-Stokes (RANS) solution algorithm for parabolic velocity fields with turbulence properties obtained using the SSG second order closure [44] to a transported PDF approach closed at joint-scalar level [16]. The latter is here extended to include the full sectional soot model, such that the joint-scalar PDF can be expressed as $\widetilde{f}_{\underline{\phi}} = (\underline{\psi}; \underline{x}, t)$ where $\underline{\psi}$ expresses the fully coupled joint-scalar sample space of a random vector $\underline{\phi} = (Y_i, N_j, H)$, where Y_i are the species mass fractions, N_j denotes the number density of particles for each soot section (the mass of each soot section is defined) and

H the mixture enthalpy. The transport equation of the joint-scalar probability density function is solved using moving Lagrangian particles. Scalar mixing, including soot sections, is treated via the modified Curl's model by Janicka et al. [45], with a constant ratio of turbulent and scalar time-scale of $C_\phi = 2.3$ [37].

The method allows the inclusion of turbulence-chemistry interactions in closed form. The coupling of turbulence to radiation is facilitated via the inclusion of enthalpy as a solved scalar and an optically thin model [46] for radiative heat losses from gas phase species (H_2O, CO, CO_2 and CH_4) and soot [15]. The applied systematically reduced gas phase chemistry [15, 37] features 144 reactions, 15 solved (H, O, OH, HO_2, H_2O, H_2, O_2, CO, CO_2, CH_3, CH_4, C_2H_2, C_2H_4, C_2H_6, and N_2) and 14 steady-state species (C, CH, $^1CH_2$, $^3CH_2$, CHO, CH_2OH, CH_3O, C_2, C_2H, C_2H_3, C_2H_5, C_2HO, C_2H_2O,

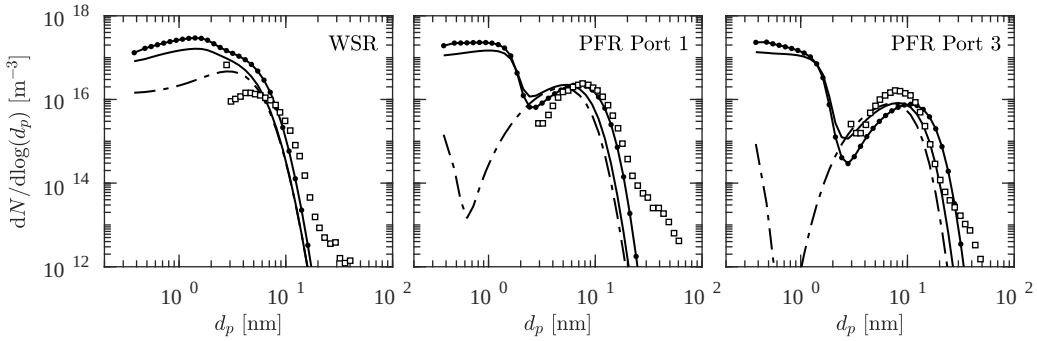

Figure 1: Soot PSDs in the WSR and at PFR Port 1 and 3 of the WSR/PFR setup of Manzello et al. [4]. Measurements by Lenhert et al. [8] shown with open squares (□), calculations using pyrene-based nucleation with dots/lines (–•–), and the acetylene-based nucleation model with solid lines (—). Dashed lines (– - –) show calculations with the lower limit collision efficiency model replaced with $\alpha_e = 1$ for acetylene-based nucleation.

and CH_2O) leading to a fully coupled solved joint-scalar space featuring 15 chemical species, 62 soot sections and enthalpy. The WSR/PFR calculations featured the detailed gas phase chemistry by Waldheim [29] comprising 359 species and 1789 reactions.

A fine grid with 500 cells in radial direction was used, with 61 cells located in the half-width of the fuel jet in the exit plane, 18 cells in the pilot zone of the burner, and the rest initially located in the co-flow. The axial grid resolution was determined at run-time according to a restrictive CFL criterion, with cells radially re-distributed in physical space as the flow develops, while

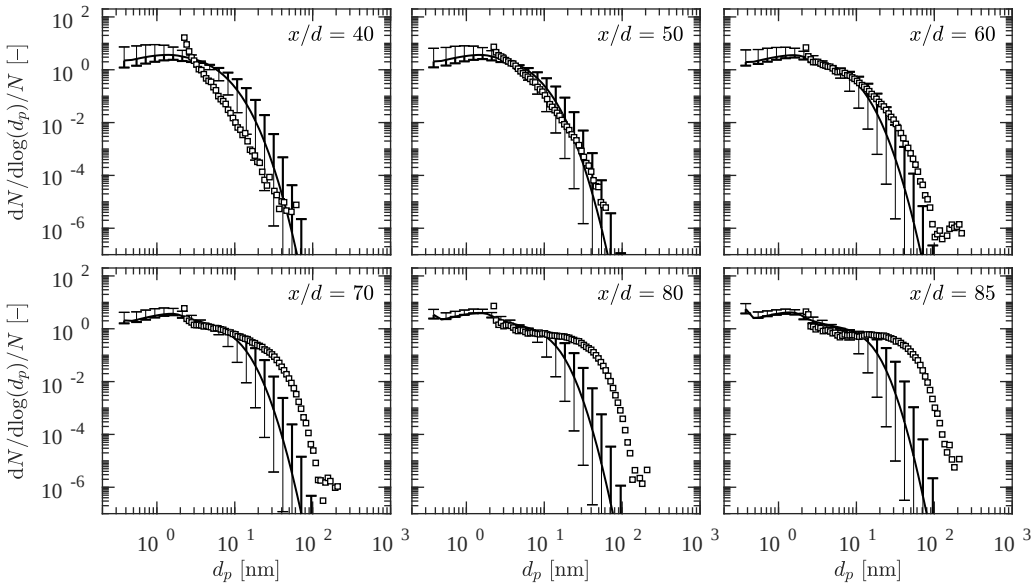

Figure 2: Normalised soot PSDs at the centreline of a C_2H_4/N_2 turbulent diffusion flame at Re = 10,000. Measurements by Chowdhury et al. [27] shown with open squares (□). Calculated soot PSDs are shown with lines (—). The impact of changing the surface reactivity parameter $\alpha_s = 0.50 \pm 0.20$ is shown with thick and thin bars, respectively. For clarity, one out of every two measured data points is omitted.

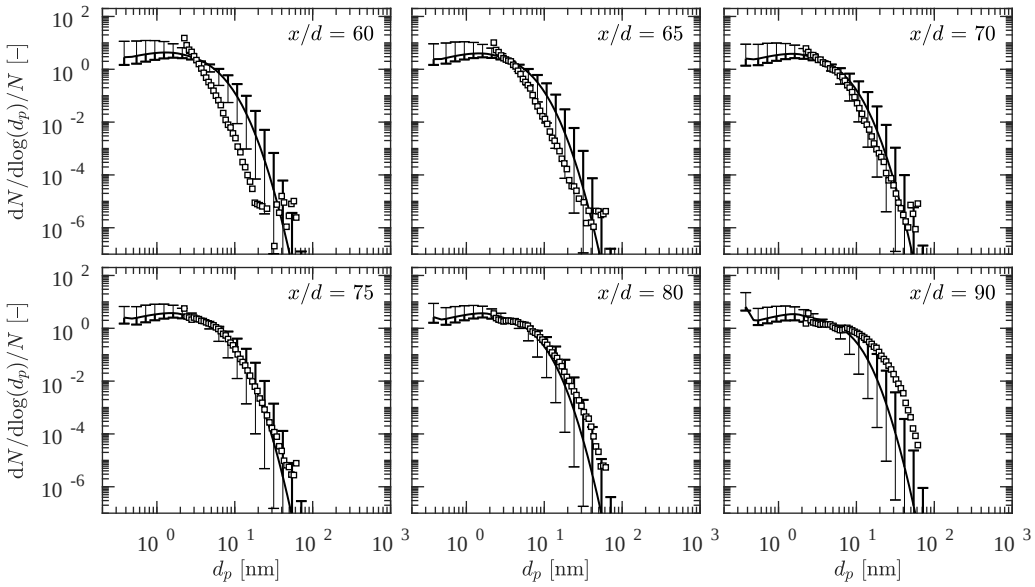

Figure 3: Normalised soot PSDs at the centreline of a C_2H_4/N_2 turbulent diffusion flame at Re = 20,000. Measurements by Boyette et al. [26] and Chowdhury et al. [27] shown with open squares (□). Calculated soot PSDs are shown with lines (—). The impact of changing the surface reactivity parameter $\alpha_s = 0.50 \pm 0.20$ is shown with thick and thin bars, respectively. For clarity, one out of every two measured data points is omitted.

keeping their position in stream function space fixed [47]. An initial number of 100 stochastic Lagrangian particles per cell was used. Results shown are independent of the grid resolution and number of particles.

2.3. Experimental Data Sets

The full sectional model was first applied to the well-stirred/plug flow reactor (WSR/PFR) configuration of Manzello et al. [4, 8] featuring a C_2H_4/air mixture at an equivalence ratio $\phi = 2.0$, close to the soot inception limit, and a temperature of 1723 K in the WSR with temperatures in the subsequent PFR following a profile descending from 1420 K to 1340 K as described by

Waldheim [29]. Boyette et al. [26] and Chowdhury et al. [27] measured PSDs in turbulent jet flames using a scanning mobility particle sizer and two nano differential mobility analysers with different size ranges. The burner design was based on that of Zhang et al. [48] featuring a C_2H_4/N_2 central fuel jet (at a volume ratio of 35/65) of diameter 3.2 mm and a concentric C_2H_4/air pilot at $\phi = 0.90$. Two sooting jet flames with Re = 10,000 and 20,000 at atmospheric pressure were investigated. In the calculations, volumetric flow rates were imposed according to Chowdhury et al. [27] with the pilot flow assumed to be at chemical equilibrium.

3. Results and Discussion

The measured and calculated soot PSDs in the WSR/PFR configuration of Manzello et al. [4, 8] are shown in Fig. 1. Results obtained with the fitted acetylene-based nucleation model, outlined above, are compared to the result obtained with the detailed pyrene-based inception chemistry of Lindstedt and Waldheim [9]. The two models agree well for the nucleation rate in Table 1. The two orders of magnitude reduction in the pre-exponential factor of the nucleation rate, compared to previous work [15, 34], is consistent with the need for a large reduction in simplified nucleation rate expressions for premixed systems identified by Faeth and co-workers [49, 50].

For $\alpha_s = 0.20$ [9] and the lower limit collision efficiency model with $D =$ 2 nm, calculations roughly match the measured PSDs in the WSR section. Agreement improves with increasing residence time, and the subsequent PFR evolution is qualitatively reproduced with the predicted peak locations for C_2H_2-based nucleation at $d_p \approx 5$ nm at Port 1 of the PFR and at $d_p \approx 8$ nm at

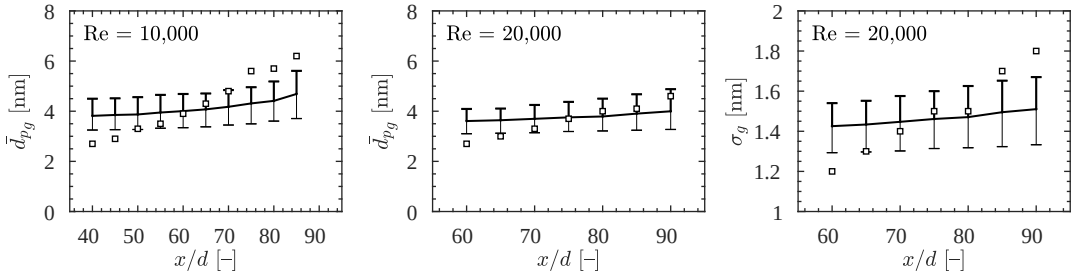

Figure 4: Geometric mean diameter ($\bar{d}_{p_g}$) of centreline PSDs in the flames at Re = 10,000 (left) and 20,000 (centre) and geometric standard deviation (σ_g) at Re = 20,000 (right). Lines and symbols as in Figs. 2–3. Experimental data by Boyette et al. [26] and Chowdhury et al. [27].

Port 3. However, larger particles ($d_p > 25$ nm) with concentrations at least two orders of magnitude below the peak are under-predicted in the PFR. While the generality of such simplified nucleation rates is questionable, the agreement is sufficient for the purpose of evaluating the evolution of PSDs in the current turbulent flames. The omission of the collision efficiency model (i.e. $\alpha_e = 1$ in Eq. (12)) leads to a pronounced depletion of small particles that is inconsistent with laminar flame data [9–12]. It was further investigated for the WSR/PFR data sets by Schiener and Lindstedt [28] and shown to occur for a wide range of nucleation rates.

Measured and calculated PSDs at the centreline of the two turbulent diffusion flames at Re = 10,000 and 20,000 are shown in Fig. 2 and 3, respectively. The PSDs are normalised using the total particle concentration (N) of all particles within the experimental detection limits (2 nm to 225 nm) in order to be consistent with the experimental procedure. The value for the surface reactivity parameter was set to $\alpha_s = 0.50$ and the sensitivity to values in the range $0.30 \leq \alpha_s \leq 0.70$ is shown. The agreement with experiment is arguably

fair overall and improved for the less sooting flame at Re = 20,000. This is perhaps surprising given the simplified nucleation rate expression applied, but also encouraging as practical applications tend to operate at higher Re numbers. Particle concentrations at the upper end of the distribution tend to be under-predicted at measurement locations further downstream. The agreement with the lower end of the measured distributions improves downstream. The measured maximum for small particles near the detection limit of the condensation particle counter (CPC) is also disproportionally affected by the algorithm correcting for diffusion losses inside the scanning mobility particle sizer (SMPS) [26, 27]. Boyette et al. [26] note that "some caution should be exercised when considering the data, especially in the range below 4 nm" and Chowdhury et al. [27] remark that "readers may choose to disregard the data for very small particles due to the large uncertainty". However, the data is included here for guidance. The applied values of α_s are somewhat higher than those used by Lindstedt and Waldheim [9] for the laminar premixed ethylene flames of Abid et al. [10–12] and the sensitivity to the parameter suggests that improved descriptions that are valid across a wider range of Lagrangian particle time histories, as encountered in different devices, remain desirable.

The sensitivity of the calculated PSDs in both flames to the model for the lower limit of the collision efficiency and model parameters was explored. The calculations shown in Figs. 2–3 use $D = 2$ nm, a value of the Hamaker constant of 7.0×10^{-20} J and $C_a = 3.0$. The value of $D = 2$ nm, marking the passing to the upper bound of the collision efficiency, is lower than applied for premixed laminar flames [9] and collision efficiencies at the lower limit

will be further decreased when a value of the Hamaker constant lower than the current 7.0×10^{-20} J is used [40, 41]. Compared to a value of $C_a = 2.2$ commonly used in moment methods [22, 35, 51], the current van der Waals enhancement factor of 3.0 will increase coagulation globally. However, only a moderate sensitivity to the replacement of the collision efficiency model with the assumption $\alpha_e = 1$ [3] or to an increased value of $D = 6$ nm was observed, and then mostly for small particles outside of the experimental data range. The impact of a decrease of the Hamaker constant to 3.0×10^{-20} J or of the van der Waals enhancement factor to $C_a = 2.2$ is even more limited. Accordingly, these results are included in the Supplemental Material.

Geometric mean diameters ($\bar{d}_{p_g}$) and standard deviations (σ_g) at Re = 20,000 [26, 27] are compared to calculations in Fig. 4. Calculations initially overpredict the measured values for $\bar{d}_{p_g} < 3.5$ nm, with improvements for larger particles, consistent with experimental uncertainties as outlined above.

Figure 5 shows scatter plots of temperature (T) and soot volume fraction (f_v) at Re = 20,000, with weighted centred moving averages also displayed. Soot is primarily present on the rich side of the stoichiometric mixture fraction ($f_{st} \approx 0.16$), with a maximum around $f = 0.25$. At $x/d = 20$, a considerable level of local extinction is apparent from the temperature distribution. The soot peak is less pronounced with relatively more soot appearing on the lean side of stoichiometry due to mixing and local extinction as compared to locations further downstream. Lindstedt et al. [42, 43] have shown that the current approach correctly predicts local extinction and reignition for turbulent non-premixed jet flames at high Reynolds numbers. Further data are included in the Supplemental Material.

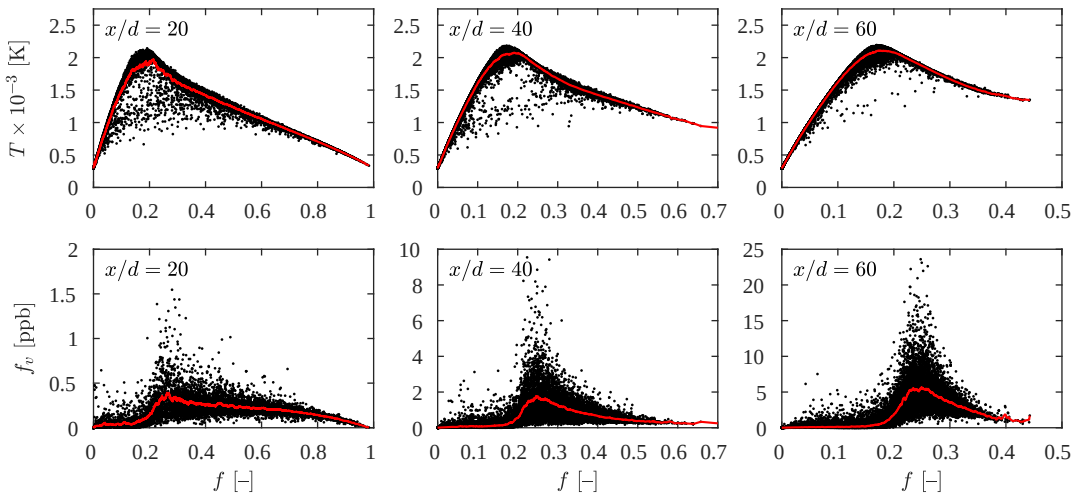

Figure 5: Scatter plots of calculated temperature (top) and soot volume fraction (bottom) at different axial locations in a C_2H_4/N_2 turbulent diffusion flame at Re = 20,000. The Lagrangian particles are shown with black dots. Red lines represent centred moving averages with a window size of 1 % of the range of mixture fraction (f) values and take particle weights into account.

4. Conclusions

Soot particle size distributions in a well-stirred/plug flow reactor setup [4, 8] and two turbulent non-premixed diffusion flames [26, 27] have been studied computationally using the combination of a mass and number density preserving sectional model and a transported PDF approach closed at the joint-scalar level. The model for the coagulation collision efficiency of small particles by Lindstedt and Waldheim [9] was included and found to improve the qualitative agreement with measured PSDs for the turbulent flames. A sensitivity study shows that the predicted PSDs in the turbulent flames are insensitive to changes of the Hamaker constant in the range 3.0–7.0 $\times 10^{-20}$ and to the van der Waals enhancement factor in the range

$C_a = 2.2$–3.0. A moderate sensitivity to the parameter D, marking the upper limit of the reduced collision efficiency model for small particles, was observed with agreement improved for $D = 2$ nm compared to 6 nm.

Calculations matched measured data well, although the treatment of the surface reactivity parameter α_s of the PAH based growth model remains a source of uncertainty. More general formulations remain desirable. The same applies to detailed and simplified models for soot nucleation. However, it also appears clear that the inclusion of the current sectional model into a transported PDF based framework for the prediction of turbulent flames enables computations of the evolution of soot PSDs with a similar accuracy to that encountered in laminar flames. The latter finding is of significant practical importance. It has also been shown that the distribution of soot in mixture fraction space is affected by local extinction events.

Acknowledgments

The authors wish to gratefully acknowledge the support of the European Union under the SOPRANO H2020 project award 690724. The data provided by Mr Wesley Boyette and Professor William Roberts from the Clean Combustion Centre at KAUST is gratefully acknowledged.

References

[1] M. D. Smooke, R. J. Hall, M. B. Colket, J. Fielding, M. B. Long, C. S. Mcenally, Combust. Theor 8 (2004) 593–606.

[2] J. Z. Wen, M. J. Thomson, S. H. Park, S. N. Rogak, M. F. Lightstone, Proc. Combust. Inst. 30 (2005) 1477–1483.

[3] J. S. Bhatt, R. P. Lindstedt, Proc. Combust. Inst. 32 (2009) 713–720.

[4] S. L. Manzello, D. B. Lenhert, A. Yozgatligil, M. T. Donovan, G. W. Mulholland, M. R. Zachariah, W. Tsang, Proc. Combust. Inst. 31 (2007) 675–683.

[5] R. P. Lindstedt, V. Markaki, R. K. Robinson, in: H. Bockhorn, A. D'Anna, H. Wang (Eds.), Combustion Generated Fine Carbonaceous Particles, KIT Scientific Publishing, Karlsruhe, 2009, pp. 499–521.

[6] D. F. Kronholm, J. B. Howard, Proc. Combust. Inst. 28 (2000) 2555–2561.

[7] R. P. Lindstedt, B. B. O. Waldheim, R. K. Robinson, in: 8th Int. Symp. Clean. Diesel Engines, Shell Global Solutions (UK), Chester, 2011, pp. 36–39.

[8] D. B. Lenhert, S. L. Manzello, Proc. Combust. Inst. 32 (2009) 657–664.

[9] R. P. Lindstedt, B. B. O. Waldheim, Proc. Combust. Inst. 34 (2013) 1861–1868.

[10] A. D. Abid, N. Heinz, E. D. Tolmachoff, D. J. Phares, C. S. Campbell, H. Wang, Combust. Flame 154 (2008) 775–788.

[11] A. D. Abid, E. D. Tolmachoff, D. J. Phares, H. Wang, Y. Liu, A. Laskin, Proc. Combust. Inst. 32 (2009) 681–688.

[12] A. D. Abid, J. Camacho, D. A. Sheen, H. Wang, Combust. Flame 156 (2009) 1862–1870.

[13] G. Narsimhan, E. Ruckenstein, J. Colloid Interface Sci. 104 (1985) 344–369.

[14] M. Frenklach, S. J. Harris, J. Colloid Interface Sci. 118 (1987) 252–261.

[15] R. P. Lindstedt, S. A. Louloudi, Proc. Combust. Inst. 30 (2005) 775–782.

[16] S. B. Pope, Prog. Energy Combust. Sci. 11 (1985) 119–192.

[17] M. Frenklach, Chem. Eng. Sci. 57 (2002) 2229–2239.

[18] J. H. Kent, D. Honnery, Combust. Sci. Technol. 54 (1987) 383–398.

[19] A. Coppalle, D. Joyeux, Combust. Flame 96 (1994) 275–285.

[20] R. McGraw, Aerosol Sci. Technol. 27 (1997) 255–265.

[21] D. L. Marchisio, R. O. Fox, J. Aerosol Sci. 36 (2005) 43–73.

[22] M. E. Mueller, G. Blanquart, H. Pitsch, Combust. Flame 156 (2009) 1143–1155.

[23] M. E. Mueller, H. Pitsch, Combust. Flame 159 (2012) 2166–2180.

[24] C. Yuan, R. O. Fox, J. Comput. Phys. 230 (2011) 8216–8246.

[25] S. Salenbauch, A. Cuoci, A. Frassoldati, C. Saggese, T. Faravelli, C. Hasse, Combust. Flame 162 (2015) 2529–2543.

[26] W. Boyette, S. Chowdhury, W. Roberts, Flow, Turbul. Combust. 98 (2017) 1173–1186.

[27] S. Chowdhury, W. R. Boyette, W. L. Roberts, J. Aerosol Sci. 106 (2017) 56–67.

[28] M. A. Schiener, R. P. Lindstedt, Combust. Theory Model. (accepted for publication 16 April 2018).

[29] B. B. O. Waldheim, Modelling of soot formation and aromatic growth in laminar flames and reactor systems, Ph.D. thesis, Imperial College London, 2015.

[30] A. Veshkini, S. B. Dworkin, M. J. Thomson, Combust. Flame 161 (2014) 3191–3200.

[31] A. Khosousi, S. B. Dworkin, Proc. Combust. Inst. 35 (2015) 1903–1910.

[32] A. Khosousi, S. B. Dworkin, Combust. Flame 162 (2015) 4523–4532.

[33] M. Frenklach, H. Wang, in: H. Bockhorn (Ed.), Soot Formation in Combustion: Mechanisms and Models, Springer-Verlag, 1994, pp. 165–192.

[34] R. P. Lindstedt, in: H. Bockhorn (Ed.), Soot Formation in Combustion: Mechanisms and Models, Springer-Verlag, 1994, pp. 417–441.

[35] A. Kazakov, H. Wang, M. Frenklach, Combust. Flame 100 (1995) 111–120.

[36] J. Appel, H. Bockhorn, M. Frenklach, Combust. Flame 121 (2000) 122–136.

[37] S. A. Louloudi, Transported probability density function modeling of turbulent jet flames, Ph.D. thesis, Imperial College London, 2003.

[38] P. Roth, O. Brandt, S. von Gersum, Proc. Combust. Inst. 23 (1990) 1485–1491.

[39] H. Guo, P. M. Anderson, P. B. Sunderland, Fuel 172 (2016) 248–252.

[40] A. D'Alessio, A. C. Barone, R. Cau, A. D'Anna, P. Minutolo, Proc. Combust. Inst. 30 (2005) 2595–2603.

[41] A. D'Anna, J. H. Kent, Combust. Flame 152 (2008) 573–587.

[42] R. P. Lindstedt, S. A. Louloudi, E. M. Váos, Proc. Combust. Inst. 28 (2000) 149–156.

[43] R. P. Lindstedt, S. A. Louloudi, Proc. Combust. Inst. 29 (2002) 2147–2154.

[44] C. G. Speziale, S. Sarkar, T. B. Gatski, J. Fluid Mech. 227 (1991) 245–272.

[45] J. Janicka, W. Kolbe, W. Kollmann, J. Non-Equilibrium Thermodyn. 4 (1979) 47–66.

[46] W. L. Grosshandler, RADCAL: A Narrow-Band Model for Radiation Calculations in a Combustion Environment., Technical Report, NIST Technical Note 1402, 1993.

[47] D. B. Spalding, GENMIX – A General Computer Program for Two-Dimensional Parabolic Phenomena, Pergamon Press, Oxford, 1977.

[48] J. Zhang, C. R. Shaddix, R. W. Schefer, Rev. Sci. Instrum. 82 (2011) 1–10.

[49] P. B. Sunderland, Ü. Ö. Köylü, G. M. Faeth, Combust. Flame 100 (1995) 310–322.

[50] P. B. Sunderland, G. M. Faeth, Combust. Flame 105 (1996) 132–146.

[51] A. Kazakov, M. Frenklach, Combust. Flame 114 (1998) 484–501.

List of Tables

List of Figures

respectively. For clarity, one out of every two measured data points is omitted.

Figure 4: Geometric mean diameter ($\bar{d}_{p_g}$) of centreline PSDs in the flames at Re = 10,000 (left) and 20,000 (centre) and geometric standard deviation (σ_g) at Re = 20,000 (right). Lines and symbols as in Figs. 2–3. Experimental data by Boyette et al. [26] and Chowdhury et al. [27].

Figure 5: Scatter plots of calculated temperature (top) and soot volume fraction (bottom) at different axial locations in a C_2H_4/N_2 turbulent diffusion flame at Re = 20,000. The Lagrangian particles are shown with black dots. Red lines represent centred moving averages with a window size of 1 % of the range of mixture fraction (f) values and take particle weights into account.

List of Supplemental Material

Supplemental material is included in form of a single PDF document, containing the following sections, tables and figures. The references in the captions below refer to the separate list of references in the supplemental document.

S1. PAH Analogy Model for Soot Surface Growth

Table S1: Reaction rate constants for the PAH analogy of soot surface chemistry [2] presented in the form $A_i \alpha_i T^{\beta_i} \exp(-E_i/RT)$. Units are in K, kmol, m^3 and s.

S2. Turbulent Flames: Sensitivities of PSDs and Scatter Plots

Figure S1: Normalised soot PSDs at the centreline of C_2H_4/N_2 turbulent diffusion flames at Re = 10,000 (top) and 20,000 (bottom). Measurements by Boyette et al. [6] and Chowdhury et al. [7] are shown with open squares (□). The original rate constant for reaction (II) [15] was used with $\alpha_s = 1.00 \pm 0.50$.

Figure S2: Normalised soot PSDs at the centreline of C_2H_4/N_2 turbulent diffusion flames at Re = 10,000 (top) and 20,000 (bottom). Measurements by Boyette et al. [6] and Chowdhury et al. [7] are shown with open squares (□). The sensitivity of the calculated PSDs (lines, —) to the replacement of the lower limit collision efficiency model with $\alpha_e = 1$ is shown with bars.

Figure S3: Normalised soot PSDs at the centreline of C_2H_4/N_2 turbulent diffusion flames at Re = 10,000 (top) and 20,000 (bottom). Measurements by Boyette et al. [6] and Chowdhury et al. [7] are shown with

open squares (□). The sensitivity of the calculated PSDs (lines, —) to an increase of the parameter $D = 2$ nm to 6 nm is shown with bars.

Figure S4: Normalised soot PSDs at the centreline of C_2H_4/N_2 turbulent diffusion flames at Re = 10,000 (top) and 20,000 (bottom). Measurements by Boyette et al. [6] and Chowdhury et al. [7] are shown with open squares (□). The sensitivity of the calculated PSDs (lines, —) to a decrease of the Hamaker constant from 7×10^{-20} J to 3×10^{-20} J is shown with bars.

Figure S5: Normalised soot PSDs at the centreline of C_2H_4/N_2 turbulent diffusion flames at Re = 10,000 (top) and 20,000 (bottom). Measurements by Boyette et al. [6] and Chowdhury et al. [7] are shown with open squares (□). The sensitivity of the calculated PSDs (lines, —) to a decrease of the van der Waals enhancement factor from $C_a = 3.0$ to 2.2 is shown with bars.

Figure S6: Scatter plots of calculated temperature, species mass fractions and soot volume fraction at different axial locations in a C_2H_4/N_2 turbulent diffusion flame at Re = 10,000. The states of the Lagrangian particles are shown with black dots. Red lines represent centred moving averages with a window size of 1 % of the range of mixture fraction (f) values, taking into account particle weight.

Figure S7: Scatter plots of calculated temperature, species mass fractions and soot volume fraction at different axial locations in a C_2H_4/N_2 turbulent diffusion flame at Re = 20,000. The states of the Lagrangian

particles are shown with black dots. Red lines represent centred moving averages with a window size of 1 % of the range of mixture fraction (f) values, taking into account particle weight.